

Millimeter-VLBI observations of low-luminosity active galactic nuclei with source-frequency phase-referencing

WU JIANG,^{1,2} ZHIQIANG SHEN,^{1,2} IVAN MARTÍ-VIDAL,³ XUEZHENG WANG,^{1,4} DONGRONG JIANG,^{1,2} AND NORIYUKI KAWAGUCHI⁵

¹*Shanghai Astronomical Observatory, Chinese Academy of Sciences, Shanghai 200030, China*

²*Key Laboratory of Radio Astronomy, Chinese Academy of Sciences, Nanjing 210008, China*

³*Department of Astronomy and Astrophysics, University of Valencia, E-46100, Burjassot, Spain*

⁴*ShanghaiTech University, 393 Middle Huaxia Road, Pudong, Shanghai, 201210, China*

⁵*National Astronomical Observatory of Japan, 2-21-1 Osawa, Mitaka, Tokyo 181-8588, Japan*

(Received Sep. 10, 2021; Revised Nov. 07, 2021; Accepted Nov. 8, 2021)

ABSTRACT

We report millimeter-VLBI results of low-luminosity active galactic nuclei (M 84 and M 87) up to 88 GHz with source-frequency phase-referencing observations. We detected the weak VLBI core and obtained the first image of M 84 at 88 GHz. The derived brightness temperature of M 84 core was about 7.2×10^9 K, which could serve as a lower limit as the core down to 30 Schwarzschild radii was still un-resolved in our 88 GHz observations. We successfully determined the core-shifts of M 87 at 22-44 GHz and 44-88 GHz through source-frequency phase-referencing technique. The jet apex of M 87 could be deduced at $\sim 46 \mu\text{s}$ upstream of the 43 GHz core from core-shift measurements. The estimated magnetic field strength of the 88 GHz core of M 87 is 4.8 ± 2.4 G, which is at the same magnitude of 1-30 G near the event horizon probed by the Event Horizon Telescope.

Keywords: LLAGN, M 84, M 87 — VLBI

1. INTRODUCTION

The low-luminosity active galactic nuclei (LLAGNs) classified by their low bolometric luminosities and sub-Eddington accretion rate commonly exist in nearby galaxies (Nagar et al. 2002; Ho 2008). Unlike their bright cousins, the broadband spectral energy distributions prefer the model of an inner advection-dominated accretion flow and an outer truncated thin disc (Yu et al. 2011; Nemmen et al. 2014). Meanwhile compact flat-spectrum radio cores were detected in LLAGNs (Nagar et al. 2002) and suggested to be scaled-down versions of AGN jets (Falcke & Biermann 1999). Hosting a large mass of central supermassive black hole and its proximity make LLAGN approachable to the launching and acceleration region of inner jet, even to its event horizon at millimeter or sub-millimeter wavelength. According to the inhomogeneous model of relativistic jet, the position of the VLBI core is frequency-dependent. This frequency-dependent shift in the location of the core (core-shift) can be used to estimate the magnetic field strength and electron number density of the jet (Lobanov 1998; Kovalev et al. 2008). However, only a few active galactic nuclei (AGNs) have reliable core-shift measurements at millimeter wavelengths (O’Sullivan & Gabuzda 2009). The core-shift measurements are mostly obtained at low frequencies due to limited sensitivity at high frequencies (Pushkarev et al. 2012). Although millimeter-VLBI can approach the inner region of jet as the plasma turns optically thin at high frequency, the core-shift is difficult to obtain due to the rapid phase fluctuations of atmosphere and thus limited coherent integration time for the conventional VLBI phase-referencing observations. Fortunately, a newly proposed VLBI phase-referencing technique called source-frequency phase-referencing (SFPR) can be used to measure the core-shift effect (Rioja & Dodson 2011), essentially being of great advantage at millimeter wavelengths. We successfully obtained the first VLBI image of the LLAGN M 81* at 88 GHz and measured the shift between 7 mm and 3 mm

wavelengths in the compact jet (Jiang et al. 2018).

In this paper, we will present the applications of SFPR to two LLAGNs, M84 and M87. The observation summary and data reduction are presented in section 2. The results are in section 3, followed by the conclusion in section 4.

2. OBSERVATIONS AND DATA REDUCTION

2.1. Observations

The observations of M84 and M87 were carried out with the VLBA in SFPR mode on June 22, 2019 with 22 and 44 GHz frequency pair. The observations with 44 and 88 GHz frequency pair were firstly performed on June 18, 2019 but most stations failed at 88 GHz. Therefore it was reobserved on March 31, 2021 for satisfied weather conditions at most stations. The on-source time of each source per scan was ~ 30 seconds at a frequency. A fast frequency-switching cycle of two frequencies on a source was taken as a loop. M87 ($\sim 1^\circ.5$ apart from M84 in the sky) was interleaved every 5 loops of M84 for the 22/44 GHz epoch and 9 loops for the 44/88 GHz epoch. Several loops of blazar 1219+044 were observed at the beginning and the end of observations but not included here, due to rapid phase fluctuations of low antenna elevation angles. The 2019 epoch was recorded at 2048 Mbps by splitting the 512 MHz total bandwidth into 16 intermediate frequency (IF) bands while the 2021 epoch was at 4096 Mbps by splitting 1024 MHz bandwidth into 8 IFs.

2.2. Data reduction

The data calibration and reduction followed the procedures in Rioja & Dodson (2011) and Jiang et al. (2018). Firstly we performed standard amplitude and phase calibrations in AIPS for both M84 and M87 at the reference frequencies (22 GHz of 2019 epoch and 44 GHz of 2021 epoch), respectively. Their images were obtained by further clean and self-calibration in Difmap. Secondly the corresponding phase solutions of the AIPS task FRING after taking into account clean models of M84 and M87 were multiplied by a factor of two, while the delay and delay rate solutions were unchanged. These revised solutions were then applied to the target frequencies (44 GHz in 2019 epoch and 88 GHz in 2021 epoch, respectively), which is called the frequency phase transfer (FPT) calibration. The phase fluctuations in proportion to the observing frequency such as the unmodeled tropospheric and geometric errors were eliminated in this step. Thirdly the SFPR-ed images of M84 at target frequencies were obtained by further phase referencing to the FRING solutions of the FPT calibrated data of M87 at the same target frequencies, which refined the unmodeled dispersive ionospheric and instrumental errors. The corresponding core-shift measurements were derived from the SFPR-ed images using JMFIT in AIPS. Finally high resolution VLBI images of M84 were obtained by clean and self-calibration in Difmap (Jiang et al. 2018).

Since the brightness-peak position of the image is usually referred as the core position, the prominent jet of M87 in right ascension (RA) direction would cause the peak position to be slightly offset from the “true core” position towards the downstream side, due to the blending of near-core jet emission within the finite beam size. To evaluate this effect, we used the method in Hada et al. (2014), the M87 structure was convolved by different beam size with diameters ranging from the minor axis of the nominal synthesized beam (shown in Table 1), whose direction was almost in RA direction in our observations, to about four times larger. Then, we plotted systematic changes of the brightness-peak position as a function of beam size. In the case of 22 GHz, the image were restored with beam sizes ranging from 0.3 to 1.2 mas in incremental steps of 0.1 mas. We found a progressive position shift of the brightness peak toward the downstream to be $10 \mu\text{as}$ per 0.1 mas in RA direction. In the case of 44 GHz, the image was restored with beam sizes ranging from 0.2 to 0.8 mas in incremental steps of 0.1 mas. The position shift of the brightness peak toward the downstream was $6.8 \mu\text{as}$ per 0.1 mas in RA direction. In the case of 88 GHz, the image was restored with beam sizes ranging from 0.15 to 0.6 mas in incremental steps of 0.05 mas. The position shift of the brightness peak toward the downstream was $2.5 \mu\text{as}$ per 0.1 mas in RA direction. That means the “true core” position would be shifted to upstream, with respect to the brightness-peak position when convolved with a nominal beam. At 22 GHz, the upstream shift in RA direction would be about $10 \times 0.39 \text{ mas} / 0.1 \text{ mas} = 39 \mu\text{as}$. At 44 GHz, it would be about $6.8 \times 0.22 \text{ mas} / 0.1 \text{ mas} = 15 \mu\text{as}$ for the 2019 epoch, and about $6.8 \times 0.24 \text{ mas} / 0.1 \text{ mas} = 16 \mu\text{as}$ for the 2021 epoch. At 88 GHz, it was about $2.5 \times 0.16 \text{ mas} / 0.1 \text{ mas} = 4 \mu\text{as}$. Where, 0.39 mas, 0.22 mas, 0.24 mas and 0.16 mas were the nominal beam sizes in the RA direction (see Table 1). Consequently, the measured core shift in RA direction from the peak-positions would be about $39 - 15 = 24 \mu\text{as}$ larger than the “true core shift” in magnitude at 22-44 GHz and, $16 - 4 = 12 \mu\text{as}$ larger at 44-88 GHz.

2.3. Error analysis

The error budgets of SFPR mainly include the dynamic tropospheric error, the core identification error of M87 and the statistical error from images. These errors are independently to each other and the total errors can be calculated as the root-sum-square of them. We adopt $11 \mu\text{as}$ for the dynamic tropospheric error among frequencies under relatively stable weather conditions, assuming 0.01 m uncanceled error by the water vapor fluctuation as that in Hada et al. (2011). The absolute tropospheric position error for a single frequency can be significantly larger than this value, while most of the error can be canceled out by the FPT calibration in SFPR observations. We also performed the error analysis for the core identification error of M87 as in Hada et al. (2011), using the core position differences between two methods. One defined the centroid of the elliptical Gaussian fitting M87 core region as the core position, the other is the brightness-peak position of the images convolved with a circular Gaussian beam of about a half of synthesized beam in the core-jet direction. The uncertainties of core identification of M87 in RA direction are $7 \mu\text{as}$, $6 \mu\text{as}$ at 22 GHz and 44 GHz for the 2019 epoch, respectively. It was $5 \mu\text{as}$, $3 \mu\text{as}$ at 44 GHz and 88 GHz for the 2021 epoch, respectively. Since the SFPR-ed images coupled the errors from both frequencies, the statistical error at each frequency was $1/\sqrt{2}$ of the beam size divided by the signal-to-noise ratios of SFPR-ed image. It was $12 \mu\text{as}$ at 22 GHz and 44 GHz for the 2019 epoch, $14 \mu\text{as}$ at 44 GHz and 88 GHz for the 2021 epoch. The intrinsic structural uncertainty of M84 would also affect the core-shift of M87. In our observations, the position angles of fitting to the core region of M84 at 22 and 44 GHz with an elliptical Gaussian were within 5 degrees in the north. Therefore the uncertainty of core-shift effect in M84 in RA direction was $5 \mu\text{as}$, $3 \mu\text{as}$ and $2 \mu\text{as}$ at 22, 44 and 88 GHz, respectively. Other minor errors such as the ionospheric residuals and geometric errors at each frequency were taken the empirical values (Hada et al. 2011). The total errors by root-sum-square all the above uncertainties give out $19 \mu\text{as}$ and $18 \mu\text{as}$ at 22 and 44 GHz for the 2019 epoch, $19 \mu\text{as}$ and $18 \mu\text{as}$ at 44 and 88 GHz for the 2021 epoch, respectively.

3. RESULTS AND DISCUSSIONS

3.1. VLBI core of M84 at 3 mm

The nearby elliptical galaxy M84 is located in the center of Virgo Cluster at a distance of 18.5 Mpc ($z = 0.00339$) and has a central supermassive black hole weighing $\sim 8.5 \times 10^8 M_\odot$. The combination of its proximity and a large black hole mass yields a privileged linear resolution conversion factor down to 1 micro-arcsecond (μas) ~ 1 Schwarzschild radii (R_S), allowing us to investigate its close vicinity of the supermassive black hole with VLBI. Two side jets are seen at a large viewing angle of $\sim 74^\circ$ (Meyer et al. 2018). The image of M84 at 88 GHz (Figure 1) was obtained by performing further clean and self-calibration in phase only to the SFPR-ed visibility data, which were scan averaged. The MODELFIT task in Difmap was used to fit the calibrated visibility with circular Gaussian components. The VLBI core of M84 could be fitted by a circular Gaussian with a flux density of $38.0 \pm 5.7 \text{ mJy}$ and a diameter of $29 \pm 11 \mu\text{as}$ well. The apparent brightness temperature of the core (Kim et al. 2018), $T_{b,app}$, can be calculated by

$$T_{b,app} = 1.22 \times 10^{12} \frac{S_{core}(1+z)}{\nu^2 \theta_{core}^2} \text{ K}, \quad (1)$$

where S_{core} is the core flux density in Jy, ν is the observing frequency in GHz, θ_{core} is the equivalent size in milli-arcsecond (mas) and z is the redshift. The $T_{b,app}$ of M84 core at 88 GHz is $\sim 7.2 \times 10^9 \text{ K}$. Similar to other LLAGNs (Kim et al. 2018), the $T_{b,app}$ is generally quite low. The derived brightness temperature could serve as a lower limit as the core size of $29 \mu\text{as}$ ($30 R_S$) was only one-tenth of the beam size and still un-resolved in our 88 GHz observations.

3.2. Core-shift of M87

M87 is the most prominent elliptical galaxy within the Virgo Cluster, located at a distance of $16.8 \pm 0.8 \text{ Mpc}$ away. Its central supermassive black hole ($\sim 6.5 \times 10^9 M_\odot$) and jet have been well-studied in almost every wave band from radio to γ -rays (Event Horizon Telescope Collaboration et al. 2019; EHT MWL Science Working Group et al. 2021). The core-shift of M87 up to 43 GHz has been measured through conventional phase-referencing to M84 (Hada et al. 2011, 2013). The core-shift in RA direction $r_{RA}(\nu)$ followed $\nu^{-0.94}$ and indicated that the black hole was located at $\sim 41 \mu\text{as}$ eastwards of the 43 GHz core (Hada et al. 2011). The core-shifts at 22-44 GHz and 44-88 GHz could be obtained from the SFPR-ed images (Rioja & Dodson 2011; Jiang et al. 2018) as shown in Figure 2. Since the jet extended structure of M84 is toward the north direction, the core-shift of M84 in RA direction could be negligible. The core-shift of M87 in RA direction could be obtained from the SFPR-ed images by Equation (2) in Jiang et al. (2018). As a result, we obtained a position shift in RA direction of $-64 \pm 8 \mu\text{as}$ at the 22 GHz core with regard to the 44 GHz core, and of $-33 \pm 11 \mu\text{as}$ at 44-88 GHz. The error in 1σ was given by JMFIT in AIPS. After taking into account of the blending

effect of near-core jet emission in M 87 (see Section 2.2), the “true core shift” would be about $-(64 - 24) = -40 \mu\text{as}$ at 22-44 GHz and $-(33 - 12) = -21 \mu\text{as}$ at 44-88 GHz. Incorporating the uncertainties given by error analysis (see Section 2.3), the core positions relative to that of the 44 GHz core in RA was $-40 \pm 19 \mu\text{as}$ at 22 GHz for the 2019 epoch and $21 \pm 18 \mu\text{as}$ at 88 GHz for the 2021 epoch, respectively.

Using the same formula $r_{RA}(\nu) = A\nu^{-k} + B$ in Hada et al. (2011), the above-mentioned two core-shifts in RA direction could be solved with solutions $A = -1.45$, $k = 0.92$ and $B = 0.045$. As presented in the bottom-right corner of Figure 3, assuming a jet position angle of -69° with respect to north in M 87 (Kim et al. 2018), B value indicates that the jet apex is located at $\sim 48 \mu\text{as}$ upstream of the 43 GHz core. It was consistent with previous result of $44 \pm 13 \mu\text{as}$ in Hada et al. (2011). Since there was no strong flare event to cause the core-shift variations (Plavin et al. 2019) during our observations as well as in Hada et al. (2011) session, it would be reasonable to align the 43 GHz core positions of M 87 among these sessions. The core-shift in RA at 22-43 GHz even during the elevated very high energy Gamma-ray state in 2012 was found to be also at a similar level ($\sim 10 \mu\text{as}$ larger) (Hada et al. 2014). Furthermore, aligning the 43 GHz cores among Hada et al. (2011) and the two epochs of this work, we fitted these combined core-shift measurements with weighted least square method. It gave out $A = -1.36 \pm 0.15$, $k = 0.92 \pm 0.06$ and $B = 0.043 \pm 0.007$ as shown in Table 2. The results are consistent and it implies the jet apex is $43 \pm 7 \mu\text{as}$ in RA (as indicated by black dashed line in Figure 3) or at $\sim 46 \mu\text{as}$ upstream of the 43 GHz core.

Following the Equation (4) in Lobanov (1998), we could estimate the core-shift measure $\Omega_{r,22-44} = 0.13 \pm 0.06$ [pc GHz] and $\Omega_{r,44-88} = 0.12 \pm 0.10$ [pc GHz], using the resultant power law index $k_r = 1.09$. The magnetic field strength at the 88 GHz core is estimated to be 4.8 ± 2.4 G using the mean value of Ω_r , by Equation (B.2) in Paraschos et al. (2021) with a spectral index of -0.5 , a Doppler factor of 2, a jet viewing angle of 18° and an intrinsic jet opening angle of $63^\circ.6$ at 88 GHz (Kim et al. 2018). This is consistent with the estimated 1-30 G near event horizon by the Event Horizon Telescope at 230 GHz (Event Horizon Telescope Collaboration et al. 2021).

4. CONCLUSIONS

We have successfully demonstrated that the SFPR technique could be applied to the mm-VLBI observations of LLAGNs. It helps to overcome the limited coherent integration time and has great advantages in detecting the weak VLBI core as well as measuring the core-shift at millimeter-wavelengths. The VLBI core of M 84 at 88 GHz was detected and the lower limit of its apparent brightness temperature $\sim 7.2 \times 10^9$ K was obtained. By means of SFPR to M 84, the core-shift of M 87 in RA direction was determined at a precision of $\sim 20 \mu\text{as}$, which further constrained the jet apex at $\sim 46 \mu\text{as}$ upstream of the 43 GHz core. With the aid of simultaneous multi-frequency receiving system and more stations available (Zhao et al. 2019; Rioja & Dodson 2020), SFPR will be a very powerful tool to investigate the compactness of the jet base at high frequencies as well as physical parameters such as core structure, brightness temperature and magnetic field of the inner region of jet.

ACKNOWLEDGMENTS

The authors thank the anonymous referee for very critical and constructive suggestions. This work was supported in part by the National Natural Science Foundation of China (grant Nos. 11803071, 11590780, 11590784, and 11933007) and Key Research Program of Frontier Sciences, CAS (grant No.QYZDJ-SSW-SLH057). VLBA is operated by the National Radio Astronomy Observatory, which is a facility of the National Science Foundation operated under cooperative agreement by Associated Universities, Inc.

REFERENCES

- | | |
|--|--|
| Event Horizon Telescope Collaboration, Akiyama, K., Alberdi, A., et al. 2019, ApJL, 875, L1.
doi:10.3847/2041-8213/ab0ec7 | Event Horizon Telescope Collaboration, Akiyama, K., Algaba, J. C., et al. 2021, ApJL, 910, L13.
doi:10.3847/2041-8213/abe4de |
| EHT MWL Science Working Group, Algaba, J. C., Anczarski, J., et al. 2021, ApJL, 911, L11.
doi:10.3847/2041-8213/abef71 | Falcke, H. & Biermann, P. L. 1999, A&A, 342, 49
Hada, K., Doi, A., Kino, M., et al. 2011, Natur, 477, 185
Hada, K., Kino, M., Doi, A., et al. 2013, ApJ, 775, 70 |

- Hada, K., Giroletti, M., Kino, M., et al. 2014, *ApJ*, 788, 165. doi:10.1088/0004-637X/788/2/165
- Ho, L. C. 2008, *ARA&A*, 46, 475.
doi:10.1146/annurev.astro.45.051806.110546
- Jiang, W., Shen, Z.-Q., Jiang, D.-r., Marti-Vidal, I., & Kawaguchi, N. 2018, *ApJL*, 853, L14
- Kim, J.-Y., Krichbaum, T. P., Lu, R.-S., et al. 2018, *A&A*, 616, A188. doi:10.1051/0004-6361/201832921
- Kovalev, Y. Y., Lobanov, A. P., Pushkarev, A. B., et al. 2008, *A&A*, 483, 759
- Lobanov, A. P., 1998, *A&A*, 330, 79
- Nagar, N. M., Falcke, H., Wilson, A. S., et al. 2002, *A&A*, 392, 53
- Meyer, E. T., Petropoulou, M., Georganopoulos, M., et al. 2018, *ApJ*, 860, 9. doi:10.3847/1538-4357/aabf39
- Nemmen, R. S., Storchi-Bergmann, T., & Eracleous, M. 2014, *MNRAS*, 438, 2804. doi:10.1093/mnras/stt2388
- O'Sullivan, S. P., & Gabuzda, D. C., 2009, *MNRAS*, 400, 26
- Paraschos, G. F., Kim, J.-Y., Krichbaum, T. P., et al. 2021, *A&A*, 650, L18. doi:10.1051/0004-6361/202140776
- Plavin, A. V., Kovalev, Y. Y., Pushkarev, A. B., et al. 2019, *MNRAS*, 485, 1822. doi:10.1093/mnras/stz504
- Pushkarev, A. B., Hovatta, T., Kovalev, Y. Y., et al. 2012, *A&A*, 545, 133
- Rioja, M., & Dodson, R., 2011, *AJ*, 141, 114
- Rioja, M. J. & Dodson, R. 2020, *A&A Rv*, 28, 6.
doi:10.1007/s00159-020-00126-z
- Yu, Z., Yuan, F., & Ho, L. C. 2011, *ApJ*, 726, 87.
doi:10.1088/0004-637X/726/2/87
- Zhao, G.-Y., Jung, T., Sohn, B. W., et al. 2019, *Journal of Korean Astronomical Society*, 52, 23.
doi:10.5303/JKAS.2019.52.1.23

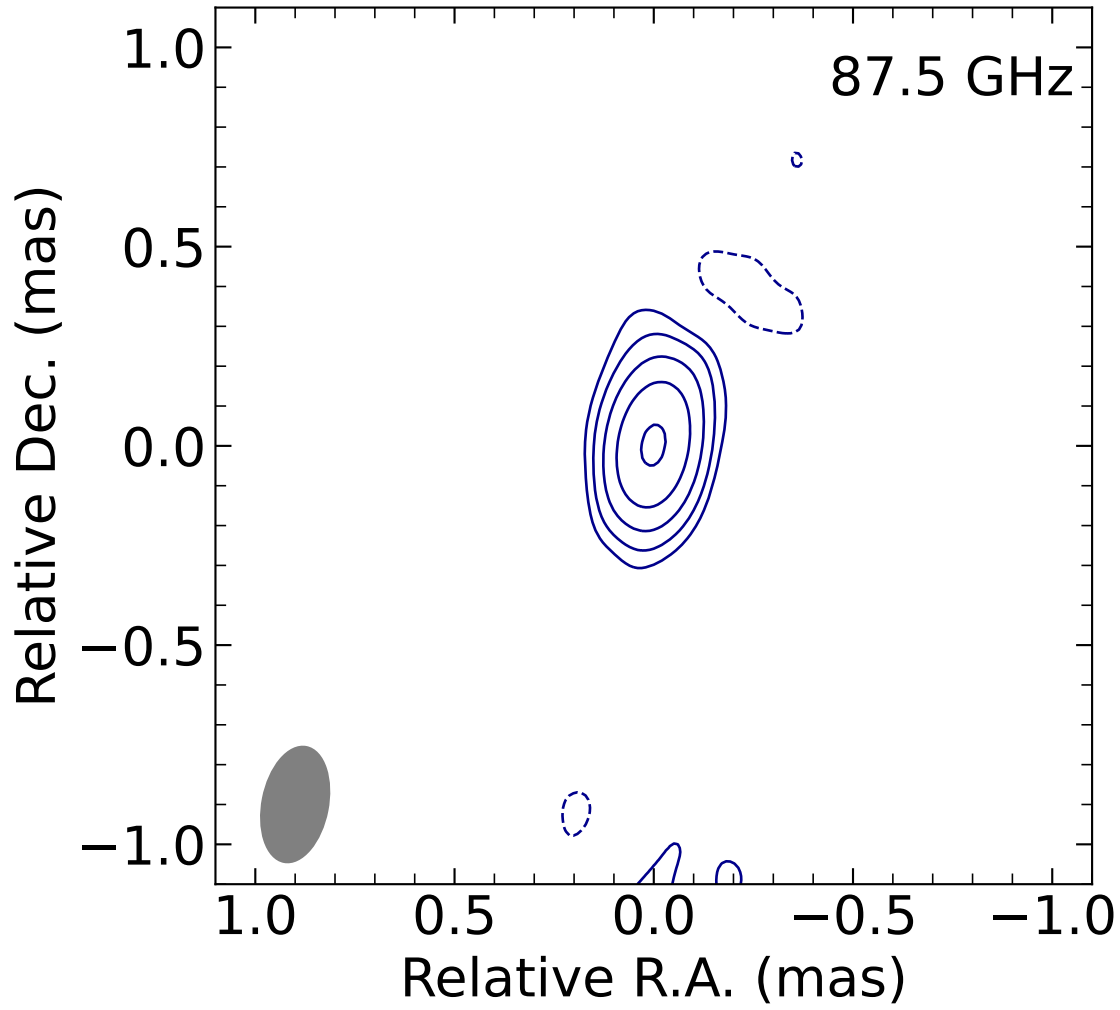


Figure 1. Natural-weighted SFPR-ed VLBI image of M84 at 88 GHz after self-calibration. The peak flux density is $38.1 \text{ mJy beam}^{-1}$. The contour levels are at $2.2 \times (-1, 1, 2, 4, 8, 16) \text{ mJy beam}^{-1}$. The lowest level is three times the rms noise of the image. The beam indicated in the left bottom corner is $0.29 \text{ mas} \times 0.16 \text{ mas}$ at -11° .

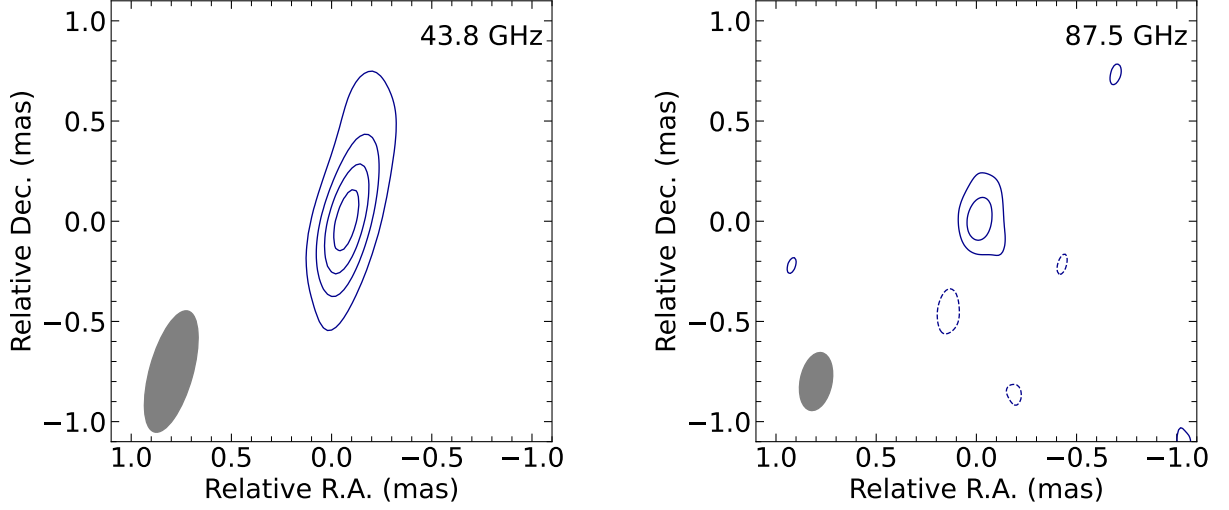


Figure 2. SFPR-ed images of M84 at 44 (left) and 88 GHz (right) on 2019 June 22 and 2021 March 31, respectively. The peak intensity is 4.1 and 8.2 mJy beam^{-1} , respectively. The contour levels are at $-3, 3, 6, 9$ and 12 times the rms of the images (0.3 and $1.0 \text{ mJy beam}^{-1}$). The full-width at half-maximum of the convolving beams ($0.63 \text{ mas} \times 0.22 \text{ mas}$ at $-15^\circ.6$ and $0.29 \text{ mas} \times 0.16 \text{ mas}$ at $-11^\circ.3$) are shown in grey at the bottom-left corners of each image.

Table 1. Summary of VLBI image parameters of M84 and M87 in the observations

No.	Epoch	Frequency GHz	Synthesized beam on M84 / M87			
			Major axis mas	Minor axis mas	Position angle degree	RA component mas
(1)	(2)	(3)	(4)	(5)	(6)	(7)
1	2019-06-22	21.9	1.49 / 1.26	0.41 / 0.37	$-14^\circ.5 / -20^\circ.5$	0.42 / 0.39
2	2019-06-22	43.8	0.63 / 0.57	0.22 / 0.21	$-15^\circ.6 / -20^\circ.4$	0.23 / 0.22
3	2021-03-31	43.8	0.60 / 0.53	0.24 / 0.22	$-18^\circ.0 / -22^\circ.7$	0.25 / 0.24
4	2021-03-31	87.5	0.29 / 0.27	0.16 / 0.15	$-11^\circ.0 / -19^\circ.6$	0.16 / 0.16

NOTE—Col.(1) Number of VLBI images at different epochs and observing frequencies; Cols.(2)-(3) Observing date and frequency; Cols.(4)-(6) The parameters (major axis, minor axis and position angle) of the nominal synthesized beam at each frequency; Col.(7) The beam size in the RA direction (RA component) of the nominal synthesized beam at each frequency.

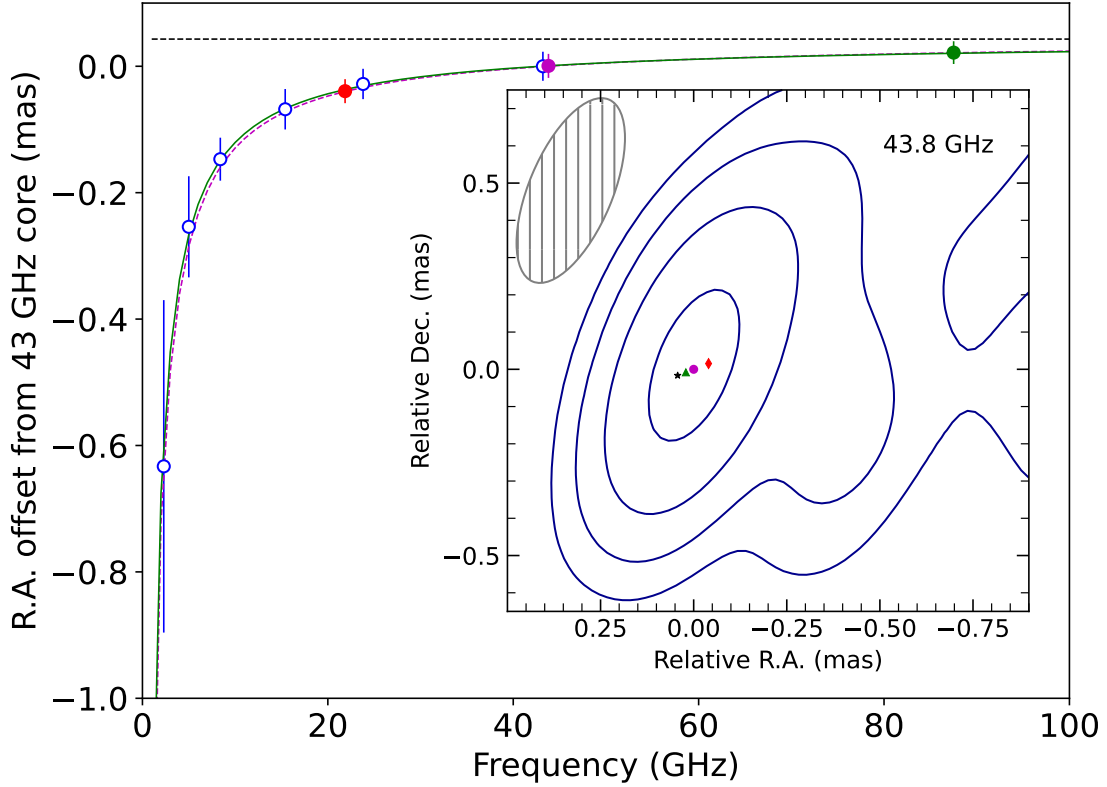


Figure 3. Offsets in right ascension (RA) with respect to observing frequency from 43 GHz core in M87. The data in hollow circles are from Hada et al. (2011). The solid circles are the measurements in this work. The fitting to the these two datasets with the same formula as Hada et al. (2011) is the green curve, indicating the jet apex position of 43 μ as in RA (black dashed line). The fitting to the data of this work only is the dashed curve in magenta. The subplot in the bottom-right corner shows the core positions at 22, 44, 88 GHz and the jet apex, which are marked as diamond, circle, triangle and star, respectively, overlapping with the VLBI image of M87 at 44 GHz in 2021. The contour levels are at 12.0 mJy beam⁻¹ (27σ noise level of the image) stepping by a factor of 3, the beam in grey is 0.53 mas \times 0.22 mas at $-22^\circ.7$.

Table 2. Fitting the location of jet apex in M87

No.	Core-shift data used	$r_{RA} = A\nu^{-k} + B$		
		A	k	B
(1)	(2)	(3)	(4)	(5)
1	this work	-1.45	0.92	0.045
2	Hada et al. (2011) and this work	-1.36 ± 0.15	0.92 ± 0.06	0.043 ± 0.007

NOTE—Col.(1) Number of the fitting; Col.(2) Core-shift measurements used; Cols.(3)-(5) Fitting parameters A , k and B . B is the offset of the jet apex in RA direction from the 43 GHz core.